J. Water Environ. Nanotechnol., 6(3): 196-211 Summer 2021

ORIGINAL RESEARCH PAPER

Fabrication of ZnO/CuO Hybrid Nanocomposite for Photocatalytic Degradation of Brilliant Cresyl Blue (BCB) Dye in Aqueous Solutions

Parmeshwar Lal Meena, Krishna Poswal and Ajay Kumar Surela

Department of Chemistry, University of Rajasthan, Jaipur (Rajasthan), India

Received: 2021-05-02 Accepted: 2021-06-05 Published: 2021-07-01

ABSTRACT

Here in the present study, we report the synthesis of ZnO nanoparticles, ZnO/CuO(3%), ZnO/CuO(5%), and ZnO/CuO(10%) nanocomposites using a simple precipitation method with the variation of CuO content and the activities of the prepared samples were investigated for degradation of Brilliant Cresyl Blue (BCB) dye under visible light conditions in aqueous solutions. The structural, morphology, optical and compositional characteristics of fabricated samples were characterized by using Fourier Transform Infra-Red (FT-IR) Spectroscopy, Field Emission Scanning Electron Microscopy combine electron dispersive spectroscopy (FESEM-EDS) and UV-vis spectroscopy. FESEM images show that ZnO nanoparticles have a polygon-like shape structure while ZnO/CuO have polygon and sheet shape structures. XRD patterns reflect the high crystallinity and purity of samples. The optical band gap values determined from the optical absorption method indicate that band gap energy decreased with the increase of CuO content in ZnO. The catalytic efficiency of the ZnO/CuO hybrid nanocomposite was observed to be higher than the ZnO nanoparticles under similar reaction conditions, 97.30% of Brilliant Cresyl Blue (BCB) dye was degraded after 100 min of irradiation of visible light radiation using the ZnO/CuO(5%) hybrid nanocomposite. The higher efficiency of ZnO/CuO compare to ZnO may be due to increased surface area and decreased bandgap energy. The kinetic study of photocatalytic degradation displayed that hybrid ZnO/CuO degraded dye with high rate constant k (34.88×10^{-3} min^{-1}) in comparison to ZnO (k, 7.00×10^{-3} min^{-1}). Reaction conditions optimization of the photodegradation process was attained by the variation in reaction factors such as pH, dye concentration, catalyst amount, and reaction time.

Keywords: *Nanocomposite, photodegradation, pollutants, semiconductor*

How to cite this article

Lal Meena P., Poswal k., Kumar Surela A. Fabrication of ZnO/CuO Hybrid Nanocomposite for Photocatalytic Degradation of Brilliant Cresyl Blue (BCB) Dye in Aqueous Solutions . J. Water Environ. Nanotechnol., 2021; 6(3): 196-211.
DOI: 10.22090/jwent.2021.03.001

INTRODUCTION

In the last few decades, environmental problems have increased tremendously due to the extensive growth in industrial and urbanization activities, and the fast growth rate of the population. Environment pollutions including water pollution worldwide become a rigorous environmental disaster that has attracted unprecedented attention of the scientific community [1].

Industrial effluents contain various pollutants such as organic dyes, heavy metal ions, etc. Among these, organic dyes are mainly discharged from the textile and dyeing industries, which are chemically stable and have low biodegradability, are extremely hazardous to the environment, and are highly toxic for humans, animals, and plants [2, 3, 4]. Thus, it is very much essential to discard these compounds from polluted water for a safer and cleaner environment.

In recent years a variety of approaches have been used to decontaminant the water from various pollutants such as physical adsorption, photodegradation, biological degradation, etc.

* Corresponding Author Email: *parmeshwar1978@gmail.com*

Among this photocatalysis, using semiconductor materials as catalysts (mainly metal oxides such as TiO_2, SnO_2, CuO, and ZnO) is considered the most attractive and viable way to resolve the critical issue of water pollution, because of its eco-friendly nature, cost-effective, long life span and it completely degrade pollutants into non-hazardous products. [5-8].

ZnO and TiO_2 are well-liked metal oxide semiconductor materials that have drawn much attention due to their higher thermal stability, photosensitivity, and non-toxicity [9]. ZnO is an n-type direct wide bandgap (Eg = 3.2 – 3.4 eV) semiconductor nanomaterial that has been extensively studied by researchers because of its eco-friendly nature, ease to synthesize, and inexpensive, and it could generate photo-excited holes with the strong oxidizing ability [10, 11]. However, major shortcomings associated with ZnO such as the large bandgap that reduces effective absorption of visible light and easy recombination of photogenerated electron-hole pairs [12-14], impede their performance as photocatalysts.

Several approaches have been employed to tailor the physical and chemical properties, and trounce these limitations by which their performance can be boosted, mainly doping of ion, deposition of noble metals (Ag, Au, or Pt), coupling of narrow bandgap semiconductor metal oxides, and metal sulfides [15,16, 17]. The combination of different nanostructured semiconductor materials in the form of nanocomposites enhances the performance by mutual separation/transfer of charge carriers (electrons and holes) from one semiconductor to other that reduces the rate of electrons and holes recombination process [18].

Various types of narrow band gap metal oxide semiconductor nanoparticles such as CuO [19-21], NiO[22] Fe_2O_3 [23], Nb_2O_5 [24], Bi_2O_3 [25], Ag_2O [26, 27] , SnO_2[28], TiO_2 [29], In_2O_3[30], WO_3[31] and sulphides like CdS[32, 33], CuS[34], ZnS[35] etc. have been coupled with ZnO to produce nanocomposites with improved characteristics.

Among these copper oxide (CuO) is a narrow bandgap (Eg =1.2 eV) p-type semiconductor that is widely employed in photocatalytic and catalytic applications, solar cells, and electrochemical fields [36-37]. And it has strong visible absorption, able to increase the transfer rate of charge carriers, and slow down the recombination electrons and holes [38-39].

Therefore, hybrid nanocomposite semiconductor system the rate of electron-hole pairs recombination decrease due to the separation of electron-hole pairs, and the reduction and oxidation reactions occur at two different reaction sites that increase the photocatalytic efficiency of semiconductors.

Thus, several studies have been reported that photodegradation of various organic dyes using ZnO/CuO hybrid nanocomposite under UV and visible light illuminations. However, the photocatalytic performance of the ZnO/CuO hybrid nanocomposite entails being improved.

Herein we report the synthesis of hybrid ZnO nanoparticles and ZnO/CuO hybrid nanocomposites by a facile and cost-effective wet precipitation technique.

The structural, morphology, optical and compositional properties of ZnO nanoparticles and ZnO/CuO hybrid nanocomposites were evaluated using several techniques such as XRD, FESEM, EDS, FTIR, and UV visible spectroscopy. The photocatalytic efficiency of synthesized samples was measure and investigated to degrade BCB dye under visible light irradiation and results were discussed. The photocatalytic performance of the ZnO/CuO hybrid nanocomposite was reported higher to compare to ZnO nanoparticles and suitable reasons were proposed to explain the improved efficiency of ZnO/CuO hybrid nanocomposite.

MATERIALS AND METHODS

Materials

Zinc acetate dihydrate ($Zn(CH_3COO)_2.2H_2O$), potassium hydroxide (KOH), copper acetate monohydrate ($Cu(CH_3COO)_2.H_2O$), N, N, N, N-Cetyl trimethylammonium bromide (CTAB), ethyl alcohol, and Brilliant Cresyl Blue (BCB) were used. All chemicals were of analytical grade and used without any further purification.

Preparation of ZnO nanoparticles

For the synthesis of ZnO nanostructures, in a typical method, 0.05 mole of $Zn(CH_3COO)_2.2H_2O$ and 3 mL of CH_3COOH dissolved in 100 mL of double distilled water with constant magnetic stirring for 30 min., then 1 gm of CTAB was added and stirred again for 60 min. Further, the pH of the solution was set up at 11 by adding 2M of KOH solution dropwise under constant stirring and the temperature of the mixture was increased to 75°C, a viscous white precipitate appeared

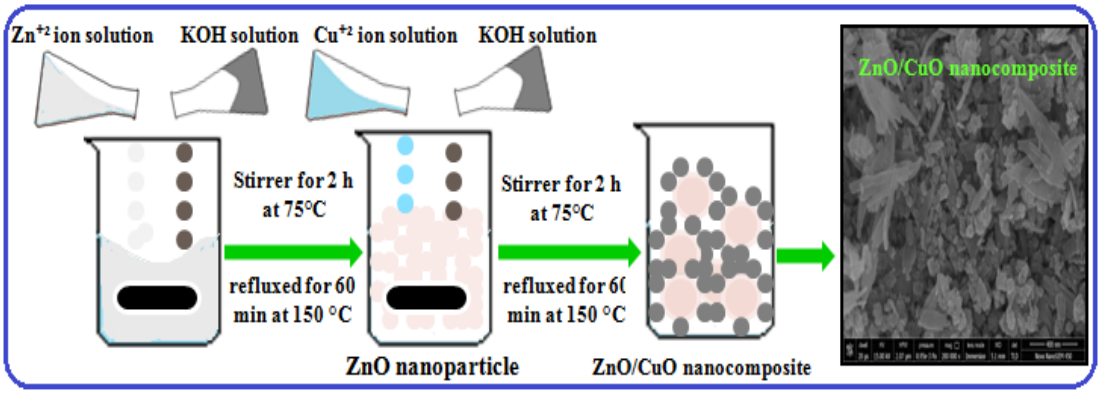

Fig.1. Schematic illustrations of synthesis procedure for ZnO/CuO nanocomposite

which was continuously stirred for 2 hours at 75°C. Afterward, the obtained white precipitated was refluxed for 1 hour at 150°C. The suspension was kept uninterrupted overnight and allowed to cool down naturally to room temperature. The white precipitate was recovered by centrifugation and repeatedly washed with double distilled water and ethyl alcohol, and dried for 5 h in a hot air oven at 85 °C temperature. The obtained white powder was used for characterization and photocatalytic studies of organic dye.

Reactions

$$Zn^{2+} + 2OH^- \longrightarrow Zn(OH)_2 \quad (1)$$

$$Zn(OH)_2 \longrightarrow ZnO + H_2O \quad (2)$$

Preparation of ZnO/CuO hybrid Nanocomposite

For fabrication of ZnO/CuO(50%) hybrid nanocomposite, 1gm of as-synthesized ZnO nanoparticles were dispersed in 100mL of distilled water and magnetically stirred for 2 hours to homogenize in water. 0.0063 mol of $Cu(CH_3COO)_2.H_2O$ dissolved in 50 mL of distilled was added dropwise under constant stirring, the mixture was further stirred continuously for 2 hours and temperature increased to 75°C, the solution converts into blue-white color due to adsorption of Cu^{2+} ions on the surface of ZnO nanoparticles. Then, the pH of the solution increased to 11 with 2M KOH solution, blue-white nanoparticles turn into blue color due to formation of $Cu(OH)_2$ on the surface of ZnO and finally convert into grey color on further stirring for 2 hours at 75°C heating. After that, the mixture was reflux at 150°C for 60 min. The mixture was kept uninterrupted overnight with mother liquor and allowed to cool down naturally to room temperature, then centrifuged, washed repeatedly with water and ethyl alcohol, and dried in an oven at 85°C for 5 hours. Similarly, ZnO/CuO (3%) and ZnO/CuO (5%) hybrid nanocomposites were prepared using appropriate quantities of copper acetate. The prepared grey-colored ZnO/CuO hybrid nanocomposites were used for characterization and photocatalytic studies of organic dye. The synthesis procedure for ZnO/CuO nanocomposite is represented schematically in **Fig. 1**.

Reactions

$$ZnO + Cu^{2+} \longrightarrow ZnO/Cu^{2+} \quad (3)$$

$$ZnO/Cu^{2+} + 2OH^- \longrightarrow ZnO/Cu(OH)_2 \quad (4)$$

$$ZnO/Cu(OH)_2 \longrightarrow ZnO/CuO + H_2O \quad (5)$$

Characterization techniques

The fabricated samples were characterized by various techniques. The crystal phases and lattice parameters of the samples were determined using X-ray diffraction (XRD) spectroscopy, while their morphology, shape, and size were estimated using field emission scanning electron microscopy (FESEM). UV-Vis spectra were recorded using a spectrophotometer over the wavelength range of 200 to 800 nm and used for assessing optical properties. Fourier-Transform Infrared (FTIR) spectra were recorded to analyze the type of bonding and functional groups in the range of 400 – 4000 cm^{-1}. The elemental composition was determined from electron dispersive spectroscopy (EDS).

Studies of Photocatalytic Activities

The photocatalytic actions of synthesized samples were inspected using Brilliant cresyl blue (BCB) dye as the model water pollutant

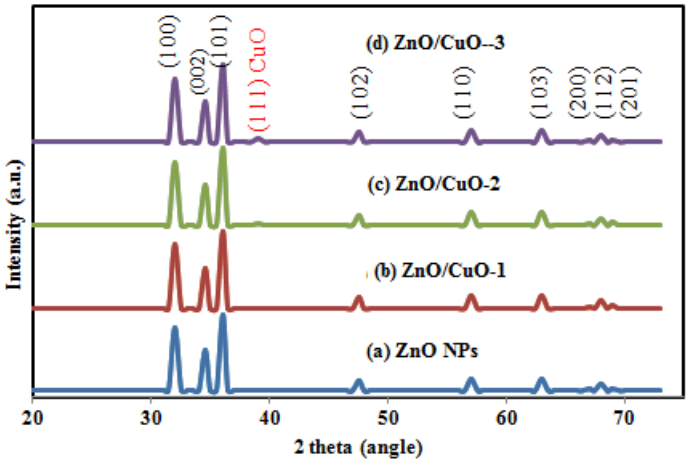

Fig.2. XRD patterns of (a) bare ZnO NPs and (b) to (d) ZnO/CuO hybrid nanocomposites

in aqueous media. The reaction conditions of experiments were optimized by the variation in pH of the reaction solution, amounts of catalyst and concentration of dye, and reaction time. The photocatalysis experiment was carried out under the irradiation of a 250 W sodium vapor lamp in a photoreactor in which the lamp was 10 cm away from the dye solution level. To achieve adsorption-desorption equilibrium of BCB on the surface of photonanocatalyst the dye solution under ambient conditions was put in dark and magnetically stirred for 30 min.

After that, the mixture was exposed to visible light in photoreactor under constant stirrer and 5 mL of dye solution was removed in predetermined time intervals, centrifuged for removal of photonanocatalyst and to determine to the residual concentration of dye in solution the absorbance was measured using a UV-visible spectrophotometer with a quartz cuvette with an optical length of 10 mm. To assess the self-degradation of dye standard experiments without using photonanocatalyst were also carried out at similar reaction conditions. The degradation percentage of BCB was calculated using the equation as given follow equation (1)

$$\text{Degradation efficiency}(\%) = \frac{C_0 - C_t}{C_0} x100 = \frac{A_0 - A_t}{A_0} x100 \quad (1)$$

Where C_0 and C_t are the initial concentration at adsorption-desorption equilibrium and after a period of irradiation, while A_0 and A_t are the absorbance of dye solutions after adsorption-desorption equilibrium and after irradiation of different time intervals.

RESULTS AND DISCUSSION

Structural analysis

XRD patterns of synthesized ZnO and ZnO/CuO nanocomposites with varied amounts of CuO are illustrated in **Fig. 2**. In the XRD patterns, characteristic diffraction peaks of hexagonal wurtzite ZnO are displayed. The XRD peaks at 2 è ≈ 31.80°, 34.54°, 36.30°, 47.57°, 56.66°, 62.94°, 66.44°, 67.92° and 69.20° correspond to the (100), (002), (101), (102), (110), (103), (200), (112) and (201) crystal planes and hexagonal crystal geometry according. The average crystallite size was estimated using Debye–Scherer relation [40] as given below (2):

$$D = \frac{K\lambda}{\beta \cos\theta} \quad (2)$$

where D is the crystallite size of the particle, K represents the Scherrer constant, which is equal to 0.9, λ is the wavelength of light used for diffraction, λ= 1.54 A°, β is the FWHM (full width at half maximum) of the diffraction peak and θ is the angle of reflection [40]. The average size of the ZnO NPs calculated from the XRD pattern was 28 nm to 55 nm, while for CuO/ZnO nanocomposite it is 18nm to 40nm approximately. CuO/ZnO nanocomposites displayed a very minor peak at 38.8°, which was indexed to the (111) of CuO [42] is appeared with the addition of Cu in ZnO. The intensity of the diffraction peak of CuO (111) was found to increase with the increase of copper content in CuO/ZnO nanocomposites. In addition,

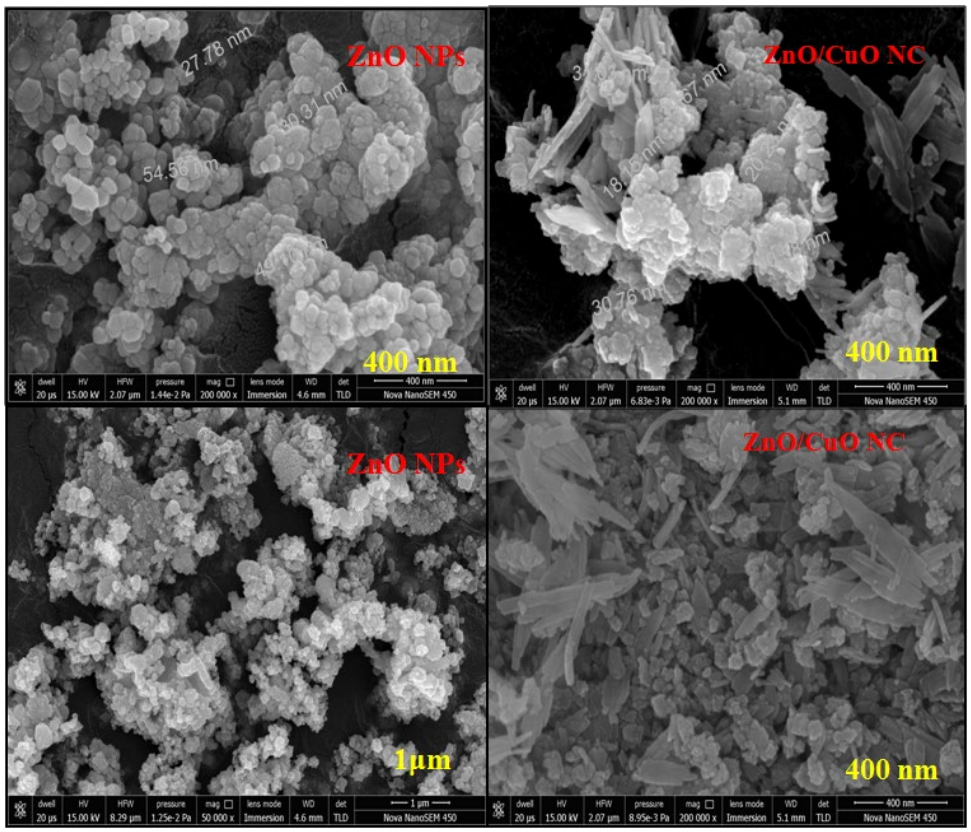

Fig.3. SEM images of prepared samples (a) ZnO (b) ZnO/CuO nanocomposite

with increased amounts of copper, no other peaks or appreciable shifts were observed and no solid solution was formed in between ZnO and CuO.

Morphological and elemental analysis

The surface morphology of the synthesized samples was inspected using an SEM connected with an X-ray for semi-quantitative elemental compositions. The FESEM images of bare ZnO nanoparticles and ZnO/CuO hybrid nanocomposites are illustrated in **Fig. 3**. As shown in FESEM images of bare ZnO nanoparticles have polygonal or disk-like shapes with little agglomerations, while ZnO/CuO nanocomposites have both sheet and polygonal or disk-like shapes. These agglomerations could be attributed to the high tendency of NPs to form large clusters. On the other hand, EDS analysis confirmed the successful synthesis of CuO, ZnO, and their composites with different ZnO/CuO ratios.

The EDS spectra representing in (**Fig. 4a** and **Fig. 4b**) showing the chemical composition of samples, confirm the existence of Zn, Cu, and O elements on the samples, and their percentage composition is shown in Table 1. Results show the presence of three elements Zn, Cu, and O within ZnO/CuO nanocomposite, whereas, pure ZnO contains only two elements: Zn and O. No other peak related to any other element was detected in the spectrum within the detection limit, which confirmed that synthesized materials were composed of Zn, Cu, and O only.

Fourier-Transform Infrared (FTIR) spectra

FTIR spectra for the synthesized samples are shown in **Fig. 5**, the strong absorption peaks in FTIR spectra observed in the range of 3424-3430 cm^{-1} indicate the existence of O-H stretching vibration of H_2O water molecules. The peaks reported between 1327-1630 cm^{-1} show the presence of CO_2 molecules absorbed by samples.

The absorption peaks that appeared within 400–650 cm^{-1} represent the metal-oxygen bonds [43]. The peak around 442 cm^{-1} (**Fig. 5a)** indicates the Zn-O stretching vibration [44], on mixing of CuO it is get shifted toward a higher wavenumber in the ZnO/CuO nanocomposites (**Fig. 5b-d**) demonstrating the integration of CuO crystal with

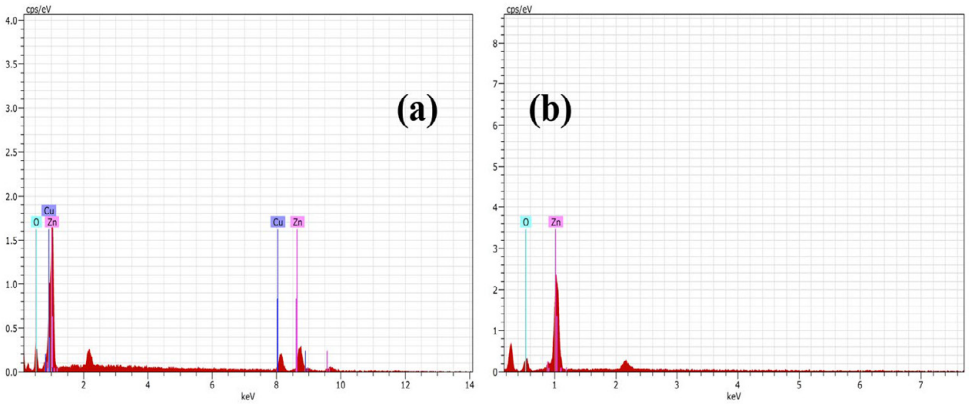

Fig.4. EDS images of (a) ZnO/CuO-3 nanocomposite (b) ZnO nanoparticles

Table.1. Elemental composition in synthesized ZnONPs and ZnO/CuO-3 nanocomposite

Nanomaterials	Element	Atom wt%	wt%
ZnO	Zn	63.56	3.40
	O	36.44	2.53
ZnO/CuO	Zn	44.98	1.39
	Cu	36.04	1.10
	O	18.98	0.84

ZnO nanoparticles [43]. The band appeared around 606 to 616 cm^{-1} as shown in (**Fig.5 b-d**) represents to Cu-O stretching vibration. The intensity of Cu–O stretching vibration appeared around 606 to 616 cm^{-1} gradually increased with the increase of Cu content in ZnO nanoparticles [45].

Optical properties

To analyze the optical properties of prepared bare ZnO-NPs, and ZnO/CuO nanocomposites, UV–vis absorption spectra with different compositions were recorded as shown in **Fig. 6a** to **Fig. 6d**. Pure ZnO exhibits strong absorption spectra at 368 nm while in ZnO/CuO nanocomposite absorption spectra the absorption bands are noticed at 372 nm and 374 nm. The integration of CuO with ZnO red shifted the maximum absorption wavelength due to increased surface defects and oxygen vacancies.

The bandgap is calculated by extrapolation the linear portion of the Tauc plot between $(\alpha hv)^2$ vs. hv to cut on the energy axis (**Fig. 6 e-h**). The bandgap energy values for fabricated bare ZnO NPs and ZnO/CuO hybrid nanocomposites were calculated by using below given equation (3).

$$(\alpha hv)^{1/n} = A(hv - E_g)$$

where α is the absorption coefficient, hv represents the energy of the photon, A is the proportionality constant and varies with the material, and n represents the index or optical transition of semiconductors, n=1/2 or 2 for direct or indirect bandgap semiconductors [46]. α was calculated by using formula $\alpha = 2.303(A)/t$, where, A is absorbance and t is the thickness of the sample. Eg is the band gap of samples that were obtained by extrapolation of the linear part of the curves at α = 0 to the energy axis (hv). Calculated band gap energy values and maximum absorbance for bare ZnO NPs and ZnO/CuO hybrid nanocomposites are represented in Table 2.

The palpable variation in band gap values verifies the interaction between ZnO and CuO which leads to the formation of mixed composites. In the hybrid nanocomposite, several energy levels exist between CuO and ZnO, and defects on the ZnO surface facilitate the interfacial transfer of photogenerated electrons and holes and decline the

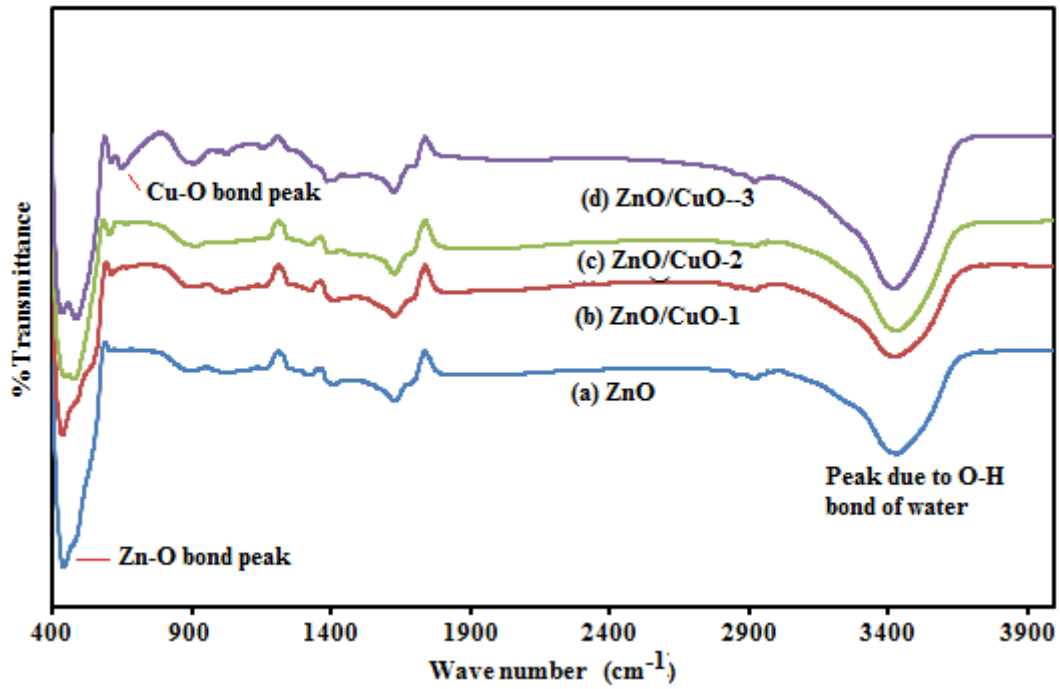

Fig.5. FTIR spectra of the prepared samples (a) ZnO nanoparticles (b) to (d) ZnO/CuO nanocomposites

recombination rate. As a result, the photocatalytic activity of ZnO/CuO hybrid nanocomposite increased as compare to ZnO [47].

Photocatalytic activity

The photocatalytic efficiency of synthesized nanocomposites was studied under visible light irradiation. To investigate photocatalytic efficiencies of as-prepared photocatalysts, 100mL of dye solutions have 15mg/L dye concentration and 15mg/100mL of catalyst doses were irradiated under visible light at optimized pH in a photoreactor. The degraded amount of BCB dye was measured by recording UV visible absorption spectra at 624nm. As shown in **Fig. 7a** the attributed absorption peak of BCB dye at 624 nm is continuously declining with time due to the photodegradation of BCB dye into non-hazardous products. In 100 min of visible light irradiation, the dye is about to completely degraded and there was no absorption peak recorded in results. The photocatalytic performance of bare ZnO and all ZnO/CuO hybrid nanocomposite materials with various compositions were also investigated.

From the results, it is attributed that hybrid nanocomposite performed better photocatalytic activity as compared to bare ZnO. However, ZnO/CuO hybrid nanocomposite material with higher and extremely lower CuO content degraded dye less effectively and maximum degradation efficacy was evidenced for ZnO/CuO (5%). To investigate the effect of catalyst alone and light alone the controlled experiment were also performed and it is established that there is a minimum self-degradation of dye. **Fig. 7a** shows photodegradation of BCB using various composites having different Zn/Cu ratios.

Low CuO concentration reduces charge transfer [48]. Further increase of CuO content in hybrid nanocomposite increase the rate of charge transfer and reduced the recombination rate of electrons and holes that increase photodegradation efficacy and at optimized CuO concentration the rate of charge transfer is substantially diminished the recombination rate of electrons and holes, as a result, the photocatalytic activity of ZnO/CuO (5%) nanocomposite was recorded highest [49, 20] and the further increase of CuO concentration wraps the lively sites on the surface of ZnO that reduces the photocatalytic activity of ZnO/CuO [48].

Effect of reaction parameters on photocatalysis

Effect of dye solution pH

The rate of photodegradation of dye solution in aqueous medium significantly varies with pH

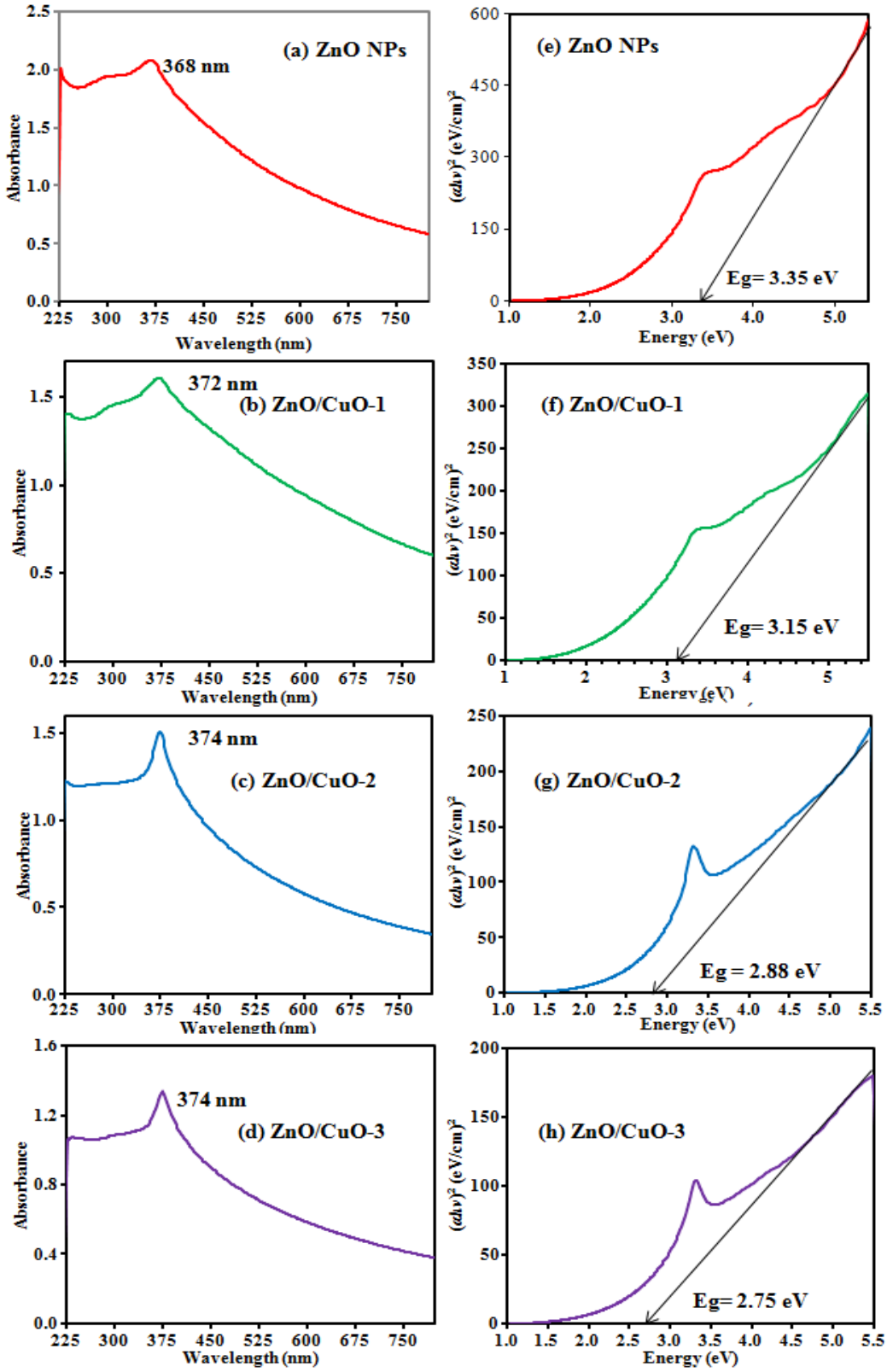

Fig.6. UV-visible absorption spectra of (a) ZnO nanoparticles and (b) to (d) ZnO/CuO nanocomposites and Tauc plots for (e) ZnO NPs and (f) to (h) ZnO/CuO nanocomposites

Table.2. Optical parameters for prepared samples

Type of nanomaterial	Maximum absorbance (nm)	Calculated band gap energy (eV)
ZnO NPs	368	3.35
ZnO/CuO-1	372	3.15
ZnO/CuO-2	374	2.88
ZnO/CuO-3	374	2.75

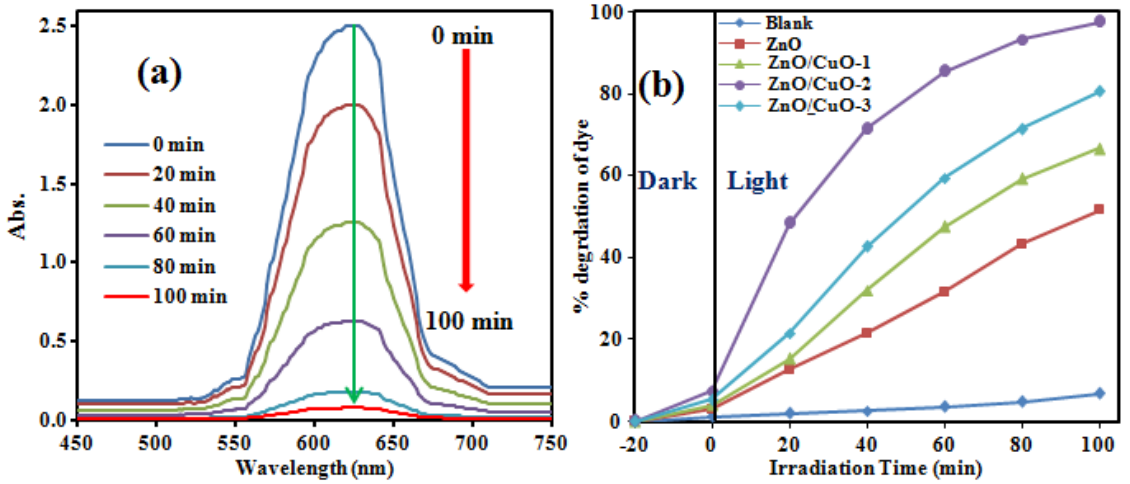

Fig.7. (a) UV–vis absorption spectra showing degradation of Brilliant cresyl blue (BCB) with ZnO/CuO nanocomposite (b) The % degradation of BCB dye by ZnO NPs and ZnO/CuO nanocomposite

value, on altering medium of dye solution (pH value) photodegradation rate changes efficiently. It is due to a change in the interaction between catalyst and dye at different pH values. For the photodegradation process of BCB dye, the effect of solution pH was investigated at different pH i.e. 5, 7, and 11 using 100mL of 15mg/L dye solution with 15mg of catalyst dose amount under visible light illumination. The results as shown in **Fig.8a** reveal that degradation rate is increasing on increasing solution pH and determined highest for pH = 11. In the acidic medium, at lower pH, the surface of the nanocomposite becomes highly positive that repels cationic dye molecules whereas in the basic medium, at higher pH the catalyst surface becomes negatively charged that significantly attracts more and more positively charged dye molecules. As a result, the rate of photodegradation increased effectively [49].

Effect of Initial Dye Concentration

The initial concentration dye also alters the rate of photodegradation. To investigate the effect of initial concentration dye the photocatalytic degradation was conducted with different initial BCB dye concentrations in the presence of CuO/ZnO, as shown in **Fig. 8b**. To evaluate the effect of dye initial concentration of 100mL of dye solutions with different concentrations varying from 5mg/L to 20mg/L and 15mg of catalyst dose were irradiated under visible light at optimized pH. From the results, as shown in **Fig. 8b,** it can be viewed that as the initial dye concentration was amplified from 5 mg/L to 25 mg/L, the dye degradation competency progressively reduced [50, 51]. The maximum degradation rate was determined with the 15 mg/L of dye concentration. And it was selected as the optimum concentration parameter to evaluate the photodegradation of dye under visible light.

Effect of Photocatalyst Dosages

To discover the optimal quantity of catalyst for the efficient photocatalytic degradation of dye, the dosages with varying amounts of catalyst from 5 to 20 mg with 15mg/L dye solutions at optimized pH were illuminated under visible

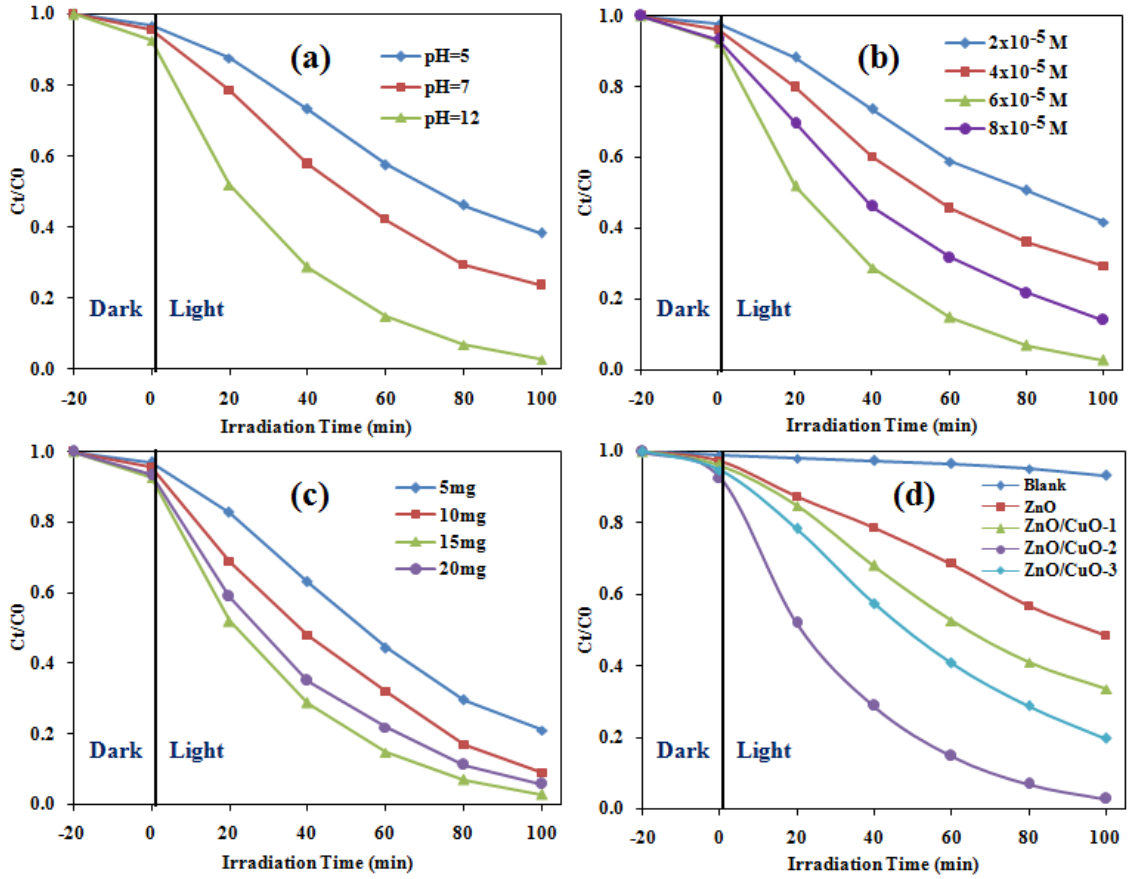

Fig.8. Effect of (a) pH values, (b) initial concentration dye, (c) dosages of photocatalyst, and (d) type of nanocomposites on photodegradation of BCB dye.

light. The degradation rate of dye was found progressively more with increasing the quantity of the catalyst as shown in **Fig.8c**. However, the highest effectiveness of catalyst was determined for 15 mg of the photocatalyst hence it was chosen optimized quantity of dose. Beyond the 15 mg level of catalyst, the efficiency was recorded constantly. The increased amount of catalyst generates more electron-hole pairs that create more active free radical species (•OH) leading to the increase of photocatalysis. Excess amount of catalyst, above the optimal amount of catalyst (15 mg), there is an increase in agglomeration of particles and decrease light infiltration through the catalyst surface due to that approach of both dye molecules and light radiation to the surface active sites of the catalyst deferred resulting into the invariable rate of photodegradation.

Kinetics of Reaction

The kinetic study of photodegradation reaction of MB dye is followed pseudo-first-order kinetics for and obeys Langmuir- Hinshelwood model expression (2)

$$\left(\ln\frac{C_t}{C_0}\right) = k_{app}t \qquad (2)$$

where C_0 is the initial concentration of dye at the equilibrium adsorption-desorption condition, C_t is the dye concentration after light illumination for time t, and, k_{app} (min^{-1}) is the degradation rate constant [52, 53].

The kinetics was investigated to draw a graph between $-\ln(C_t/C_0)$ and time (t) as shown in **Fig.9a**. It is clear from the results that the reaction rate is higher for ZnO/CuO nanocomposite compares to bare ZnO NPs. The value of rate constant k increased first with the addition of copper concentration from 3 to 5 % (0.011 min^{-1} 0.03488 min^{-1}) and then decreased by 50 % (**Fig. 9b**). This

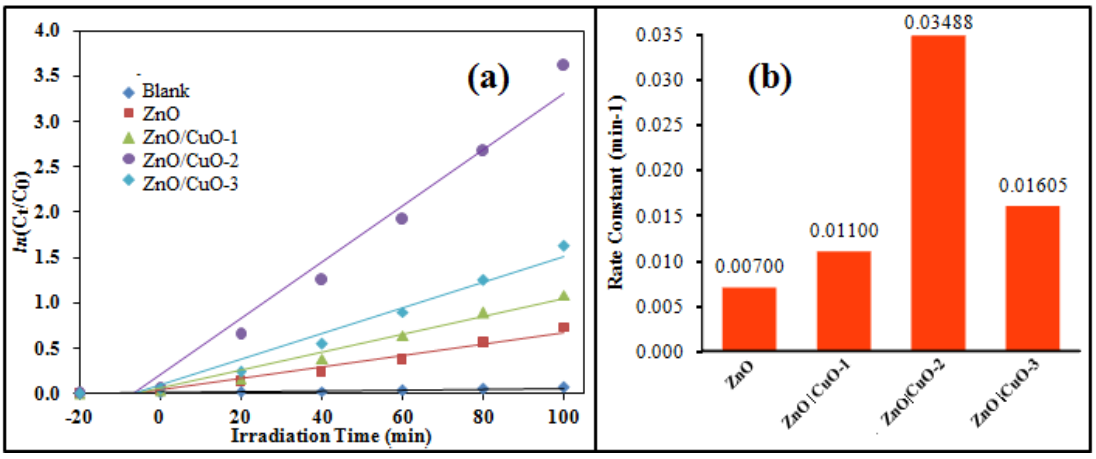

Fig.9. The plot of (a) $\ln(C_0/C_t)$ vs irradiation time (t) of BCB degradation of ZnO NPs and ZnO/CuO composites and (b) bar diagram for rate constants for BCB degradation by ZnO NPs and ZnO/CuO composites.

Table.3. Pseudo-first-order kinetics data values for ZnO NPs and ZnO/CuO nanocomposite

Pseudo first order			
Nanomaterials	Rate constant (min^{-1})	% degradation efficiency	R2
ZnO NPs	7.00×10^{-3}	51.50	0.969
ZnO/CuO-1 NC	11.00×10^{-3}	66.43	0.965
ZnO/CuO-2 NC	34.88×10^{-3}	97.30	0.964
ZnO/CuO-3 NC	16.05×10^{-3}	80.37	0.967

is as the presence of copper into the ZnO lattice improved the photocatalytic action by expanding the life span of charge carriers [21].

Rate constant, % degradation efficiency, and regression constant (R2) values of organic dye photodegradation reaction using synthesized catalysts are listed in Table 3. Among all synthesized composites, ZnO/CuO(5%) possess the highest value of the rate constant for organic dye degradation

Table 4 shows the clear comparison among the photocatalytic performance of present work as compared to some recently reported studies on ZnO/CuO nanomaterials with various organic dyes and Table 5 represents the comparison among the photocatalytic performance of various photocatalysts concerning photodegradation of Brilliant cresyl blue (BCB) dye.

Photocatalytic Degradation Mechanism

The photocatalytic degradation of BCB over ZnO/CuO nanocomposites depends on various factors such as the extent of charge separation, energy band structure, formation of p-n hetero-junction, morphology, and crystal structure of ZnO and CuO. The proposed schematic mechanism of photodegradation of organic dye via ZnO/CuO nanocomposites is shown in **Fig. 10** according to previous reports. Band edge positions of ZnO and CuO are well-situated concerning charge carrier transfer that make the charge carrier transfer process thermodynamically favorable between them and suppress the recombination rate that enhances the photoactivity of mixed ZnO/CuO nanocomposites [54]. Upon absorption of solar radiation, electrons excited from the valence to conduction band and generate holes in valence band in both ZnO and CuO semiconductor and the electrons from the conduction band of CuO transferred to the conduction band of ZnO while photoinduced holes transferred in opposite direction from valence band of ZnO to the conduction band of CuO at the interface of ZnO/CuO hetero-junction. These electrons present in the conduction band of ZnO

Table 4. Comparison of the photocatalysis results with recently reported studies

Photocatalyst	Synthesis Methodology	Dye	Efficiency	Time (minutes)	Light Source	Ref.
ZnO/CuO hybrid nanocomposite	Precipitation method	BCB	97.30%	100	Visible light (250W Na lamp)	This work
Heterogeneous ZnO/CuO nanostructures	Hydrothermal method	RHB	96.84%	100	UV light	49
CuO decorated ZnO nanoflakes	Hydrothermal method	MB MO R6G	78.9%	40	Solar light	55
ZnO/CuO hollow microspheres	Self-assembly method	RHB	93.2% 90.1%	60	Solar light	56
2D CuO-ZnO hybrid nanostructures	Wet chemical method	MB	97.80%	80	Solar light	57
ZnO/CuO nanocomposite	Sol-gel method	MB	93.8%	100	UV light	58
ZnO/CuO	Hydrothermal method	MB	93%	20	Visible light	21
CuO/ZnO nano-photocatalysts	Green method	MB	92.52%	120	500 W tungsten lamp	59
ZnO/CuO n-n heterojunction photocatalyst	Microwave assisted method	Acid orange 7	97%	5	Solar Light	60
ZnO/CuO nanocomposite	Hydrothermal method	RHB	80.50%	85	300W Xe lamp	61
ZnO/CuO nanocomposite	Simple convenient method	MO RHB	63.8%	120	400W Hg lamp	62
ZnO/CuO nanocomposite	Low temperature solution processing	CR RHB	98%	120	Tungsten lamp 10W	63

Table 5. Comparison among the photocatalytic efficiency of various photocatalysts for photodegradation of BCB dye

Photocatalyst	Efficiency	Time (minutes)	Light Source	Ref.
ZnO/CuO hybrid nanocomposite	97.30%	100	Visible light (250W Na lamp)	This work
Co_3O_4/Fe_2O_3	97%	180	Solar light	64
TiO_2	96%	480	Solar light	65
Al_2O_3	91.67%	60	Solar light	66
Al_2O_3 doped Mn_3O_4	60%	300	Solar light	67
ZnO	89%	60	125W Hg lamp	68
TiO_2	96%	480	500W halogen lamp	69

upon reacting with dissolved oxygen molecules form superoxide radicals anion ($O_2^{\cdot-}$) which further indirectly convert into reactive hydroxide radicals ($OH^{\bullet}$). Moreover, the holes in the valence band of CuO interacting with OH^- produce highly reactive hydroxyl radicals. The generated free radical species interact with dye molecules leading to the entire mineralization of dye in CO_2 and H_2O [21].

$$ZnO/CuO + h\nu \rightarrow ZnO/CuO\left(e^-_{(CB)} + h^+_{(VB)}\right) \quad (6)$$

$$ZnO/CuO\left(e^-_{(CB)} + h^+_{(VB)}\right) \rightarrow ZnO\left(e^-_{(CB)}\right) + CuO\left(h^+_{(VB)}\right) \quad (7)$$

$$ZnO\left(e^-_{(CB)}\right) + O_2 \rightarrow O_2^{\cdot-} \quad (8)$$

$$CuO\left(h^+_{(VB)}\right) + H_2O \rightarrow OH^{\cdot} + H^+ \quad (9)$$

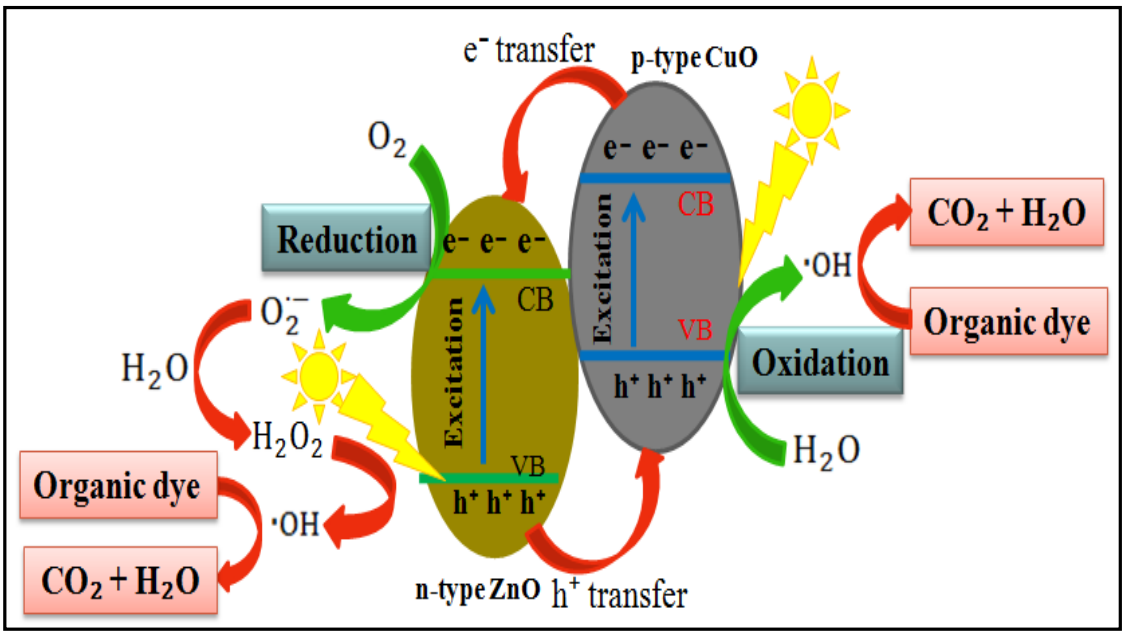

Fig.10: Mechanism of photodegradation of organic dye by ZnO/CuO hybrid nanocomposite.

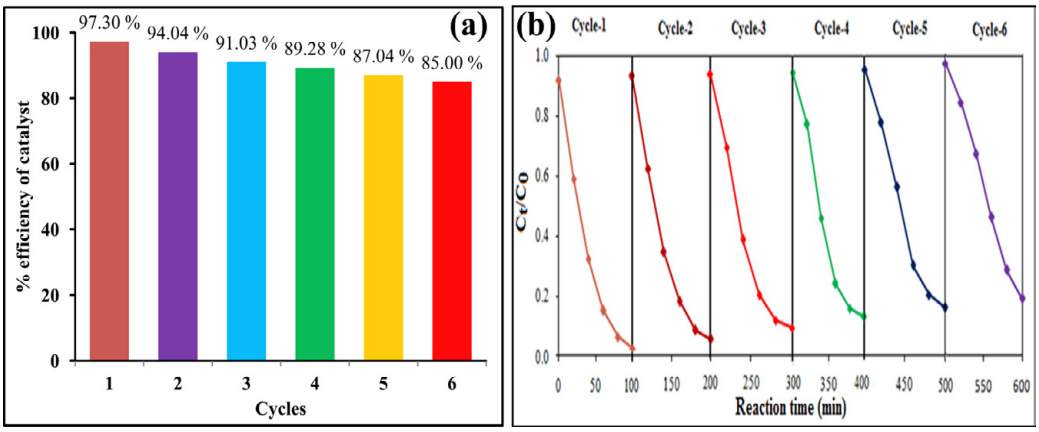

Fig.11. The efficiency of ZnO/CuO nanocomposites over continuous use in different cycles

$$O_2^{\cdot-} + H_2O \rightarrow {}^{\cdot}OOH + OH^- \quad (10)$$

$$2OOH^{\cdot} \rightarrow H_2O_2 + O_2 \quad (11)$$

$$H_2O_2 + O_2^{\cdot-} \rightarrow {}^{\cdot}OH + OH^- + O_2 \quad (12)$$

$$OH^{\cdot} + \text{dye} \rightarrow \text{Intermediates} \rightarrow H_2O + CO_2 \quad (13)$$

$$O_2^{\cdot-} + \text{dye} \rightarrow \text{Intermediates} \rightarrow H_2O + CO_2 \quad (14)$$

Reusability of the Catalyst

On the continuous use of catalyst, the effectiveness is distressed significantly. The efficacy of the prepared photocatalyst for dye photodegradation under visible light irradiation was examined in continuous use of six cycles. After use in one cycle, the catalyst was effectively separated from the reaction mixture of the photocatalysis experiments by centrifugation and reused for the next cycle and the percentage degradation efficiency was calculated. It was followed for six cycles. In the first cycle of use, CuO/ZnO showed 97.30% degradation efficiency as shown in **Fig. 11a** and for next cycles, 94.04,

91.02, 89.28, 87.04%, and 85 % degradation efficiency was obtained for second, third, fourth fifth, and sixth cycles, respectively after 100 min as illustrated in **Fig.11a** and **Fig.11b.** As results are indicating that the photocatalytic effectiveness of the synthesized ZnO/CuO nanocomposite did not decline appreciably, this reflects that the catalyst had good stability and sustainability. In the use of six cycles, the efficacy declined from 97.30% to 85%, which might be due to the adsorption of intermediate products form during degradation on the surface of photocatalyst at active sites and make them unavailable for the degradation of the fresh dye molecules.

CONCLUSION

In summary, we have been successfully fabricated pure ZnO and ZnO/CuO hybrid nanocomposite with different concentrations of CuO for sunlight-induced superior photodegradation activity of organic dye pollutant in an aqueous medium. At 5% of CuO content, ZnO/CuO hybrid nanocomposites demonstrate excellent photocatalytic activity for BCB organic dye and degraded 97.30% in 100 min. The results indicated that the presence of CuO was found to influence the photocatalytic activity of ZnO.

The FESEM studies show that ZnO NPs have polygonal or disk-like shapes with 28 nm to 55nm size while in ZnO/CuO hybrid nanocomposites both polygonal or disk-like and sheet shapes (CuO NPs) with approximately 18 nm to 40 nm size prepared. Optical absorption studies guaranteed that the bandgap narrowing and enhancement in the visible light absorption with the increase of CuO amount. The assimilation of CuO nanoparticles onto ZnO nanostructures significantly advanced the separation of charge carriers which results in the enhancement of photocatalytic efficacy.

CONFLICTS OF INTEREST

The authors declare that there are no conflicts of interest.

ACKNOWLEDGMENTS

The authors are grateful to the University of Rajasthan, Jaipur for providing the necessary facilities and support for this work.

REFERENCES

1. Wang M, Sun L, Lin Z, Cai J, Xie K, Lin C. p–n Heterojunction photoelectrodes composed of Cu2O-loaded TiO2 nanotube arrays with enhanced photoelectrochemical and photoelectrocatalytic activities. Energy & Environmental Science. 2013;6(4):1211.
2. Bhattacharjee A, Ahmaruzzaman M. Photocatalytic-degradation and reduction of organic compounds using SnO2 quantum dots (via a green route) under direct sunlight. RSC Advances. 2015;5(81):66122-33.
3. Ajmal A, Majeed I, Malik RN, Idriss H, Nadeem MA. Principles and mechanisms of photocatalytic dye degradation on TiO2based photocatalysts: a comparative overview. RSC Adv. 2014;4(70):37003-26.
4. Raliya R, Avery C, Chakrabarti S, Biswas P. Photocatalytic degradation of methyl orange dye by pristine titanium dioxide, zinc oxide, and graphene oxide nanostructures and their composites under visible light irradiation. Applied Nanoscience. 2017;7(5):253-9.
5. Fujishima A, Honda K. Electrochemical Photolysis of Water at a Semiconductor Electrode. Nature. 1972;238(5358):37-8.
6. McLaren A, Valdes-Solis T, Li G, Tsang SC. Shape and Size Effects of ZnO Nanocrystals on Photocatalytic Activity. Journal of the American Chemical Society. 2009;131(35):12540-1.
7. Sakwises L, Pisitsak P, Manuspiya H, Ummartyotin S. Effect of Mn-substituted SnO2 particle toward photocatalytic degradation of methylene blue dye. Results in Physics. 2017;7:1751-9.
8. Sonia S, Poongodi S, Kumar PS, Mangalaraj D, Ponpandian N, Viswanathan C. Hydrothermal synthesis of highly stable CuO nanostructures for efficient photocatalytic degradation of organic dyes. Materials Science in Semiconductor Processing. 2015;30:585-91.
9. Zheng Y, Chen C, Zhan Y, Lin X, Zheng Q, Wei K, et al. Luminescence and Photocatalytic Activity of ZnO Nanocrystals: Correlation between Structure and Property. Inorganic Chemistry. 2007;46(16):6675-82.
10. Sun T, Qiu J, Liang C. Controllable Fabrication and Photocatalytic Activity of ZnO Nanobelt Arrays. The Journal of Physical Chemistry C. 2008;112(3):715-21.
11. Baig, A.U., adamalar, R., Vinodhini, A., Fairose, S., Gomathiyalini, A., Begum, N. J. and Jabeen, S., 2020. Facile Green Synthesis of Silver Doped ZnO Nanoparticles Using Tridax Procumbens Leaf Extract and their Evaluation of Antibacterial Activity. J. Water Environ. Nanotechnol., 5(4): 307-320.
12. Wang J, Tsuzuki T, Sun L, Wang X. Reducing the Photocatalytic Activity of Zinc Oxide Quantum Dots by Surface Modification. Journal of the American Ceramic Society. 2009;92(9):2083-8.
13. Yang JL, An SJ, Park WI, Yi GC, Choi W. Photocatalysis Using ZnO Thin Films and Nanoneedles Grown by Metal-Organic Chemical Vapor Deposition. Advanced Materials. 2004;16(18):1661-4.
14. Lu F, Cai W, Zhang Y. ZnO Hierarchical Micro/Nanoarchitectures: Solvothermal Synthesis and Structurally Enhanced Photocatalytic Performance. Advanced Functional Materials. 2008;18(7):1047-56.
15. Gupta J, Bahadur D. Visible Light Sensitive Mesoporous Cu-Substituted ZnO Nanoassembly for Enhanced Photocatalysis, Bacterial Inhibition, and Noninvasive Tumor Regression. ACS Sustainable Chemistry & Engineering. 2017;5(10):8702-9.
16. Jonayat ASM, van Duin ACT, Janik MJ. Ab Initio Thermodynamic Investigation of Monolayer Stability of Multicomponent Metal Oxides: MxOy/ZnO(0001) and

MxOy/TiO2(110) (M = Pd, Ru, Ni, Pt, Au, Zn). The Journal of Physical Chemistry C. 2017;121(39):21439-48.
17. Karnati P, Haque A, Taufique M, Ghosh K. A Systematic Study on the Structural and Optical Properties of Vertically Aligned Zinc Oxide Nanorods Grown by High Pressure Assisted Pulsed Laser Deposition Technique. Nanomaterials. 2018;8(2):62.
18. Li B, Wang Y. Facile synthesis and photocatalytic activity of ZnO–CuO nanocomposite. Superlattices and Microstructures. 2010;47(5):615-23.
19. Lin Y-G, Hsu Y-K, Chen S-Y, Chen L-C, Chen K-H. Microwave-activated CuO nanotip/ZnO nanorod nanoarchitectures for efficient hydrogen production. J Mater Chem. 2011;21(2):324-6.
20. Kumari V, Yadav S, Mittal A, Kumari K, Mari B, Kumar N. Surface Plasmon response of Pd deposited ZnO/CuO nanostructures with enhanced photocatalytic efficacy towards the degradation of organic pollutants. Inorganic Chemistry Communications. 2020;121:108241.
21. Harish S, Archana J, Sabarinathan M, Navaneethan M, Nisha KD, Ponnusamy S, et al. Controlled structural and compositional characteristic of visible light active ZnO/CuO photocatalyst for the degradation of organic pollutant. Applied Surface Science. 2017;418:103-12.
22. Udayachandran Thampy US, Mahesh A, Sibi KS, Jawahar IN, Biju V. Enhanced photocatalytic activity of ZnO–NiO nanocomposites synthesized through a facile sonochemical route. SN Applied Sciences. 2019;1(11).
23.Liu, Y., L. Yu, Y. Hu, C.F. Guo, F.M. Zhang and X.W. Lou, 2012. A magnetically separable photocatalyst based on nest-like g-Fe_2O_3/ZnO double-shelled hollow structures with enhanced photocatalytic activity. Nanoscale, 4: 183–187.
24. Lam S-M, Sin J-C, Satoshi I, Abdullah AZ, Mohamed AR. Enhanced sunlight photocatalytic performance over Nb2O5/ZnO nanorod composites and the mechanism study. Applied Catalysis A: General. 2014;471:126-35.
25. Balachandran S, Swaminathan M. Facile Fabrication of Heterostructured Bi2O3–ZnO Photocatalyst and Its Enhanced Photocatalytic Activity. The Journal of Physical Chemistry C. 2012;116(50):26306-12.
26. Wu M, Yan J-M, Zhao M, Jiang Q. Facile Synthesis of an Ag2O-ZnO Nanohybrid and Its High Photocatalytic Activity. ChemPlusChem. 2012;77(10):931-5.
27. Kadam A, Dhabbe R, Gophane A, Sathe T, Garadkar K. Template free synthesis of ZnO/Ag2O nanocomposites as a highly efficient visible active photocatalyst for detoxification of methyl orange. Journal of Photochemistry and Photobiology B: Biology. 2016;154:24-33.
28. Wang Z, Li Z, Zhang H, Wang C. Improved photocatalytic activity of mesoporous ZnO–SnO2 coupled nanofibers. Catalysis Communications. 2009;11(4):257-60.
29.Marci, G., V. Augugliaro, M.J. Lopez-Munoz, C. Martin, L. Palmisano, V. Rives, M. Schiavello, R.J.D. Tilley and A.M. Venezia, 2001. Preparation characterization and photocatalytic activity of polycrystalline ZnO/TiO_2 systems. J. Phys. Chem. B, 105: 1026–1032.
30. Wang Z, Huang B, Dai Y, Qin X, Zhang X, Wang P, et al. Highly Photocatalytic ZnO/In2O3 Heteronanostructures Synthesized by a Coprecipitation Method. The Journal of Physical Chemistry C. 2009;113(11):4612-7.
31. Adhikari S, Sarkar D, Madras G. Highly efficient WO3–ZnO mixed oxides for photocatalysis. RSC Advances. 2015;5(16):11895-904.
32. Xu F, Yuan Y, Han H, Wu D, Gao Z, Jiang K. Synthesis of ZnO/CdS hierarchical heterostructure with enhanced photocatalytic efficiency under nature sunlight. CrystEngComm. 2012;14(10):3615.
33. Jana TK, Pal A, Chatterjee K. Self assembled flower like CdS–ZnO nanocomposite and its photo catalytic activity. Journal of Alloys and Compounds. 2014;583:510-5.
34. Cao F, Pan Z, Ji X. Enhanced photocatalytic activity of a pine-branch-like ternary CuO/CuS/ZnO heterostructure under visible light irradiation. New Journal of Chemistry. 2019;43(28):11342-7.
35. Jia W, Jia B, Qu F, Wu X. Towards a highly efficient simulated sunlight driven photocatalyst: a case of heterostructured ZnO/ZnS hybrid structure. Dalton Transactions. 2013;42(39):14178.
36. Lim Y-F, Chua CS, Lee CJJ, Chi D. Sol–gel deposited Cu2O and CuO thin films for photocatalytic water splitting. Phys Chem Chem Phys. 2014;16(47):25928-34.
37. Jang YJ, Jang J-W, Choi SH, Kim JY, Kim JH, Youn DH, et al. Tree branch-shaped cupric oxide for highly effective photoelectrochemical water reduction. Nanoscale. 2015;7(17):7624-31.
38. Fu M, Li Y, wu S, Lu P, Liu J, Dong F. Sol–gel preparation and enhanced photocatalytic performance of Cu-doped ZnO nanoparticles. Applied Surface Science. 2011;258(4):1587-91.
39. Moussa H, Merlin C, Dezanet C, Balan L, Medjahdi G, Ben-Attia M, et al. Trace amounts of Cu 2+ ions influence ROS production and cytotoxicity of ZnO quantum dots. Journal of Hazardous Materials. 2016;304:532-42.
40. Sherly ED, Vijaya JJ, Kennedy LJ. Visible-light-induced photocatalytic performances of ZnO–CuO nanocomposites for degradation of 2,4-dichlorophenol. Chinese Journal of Catalysis. 2015;36(8):1263-72.
41.Jacob, R. and J. Isac, 2015. X-ray diffraction line profile analysis of Ba0.6Sr0.4FexTi(1-x) O3-δ, (x=0.4). Int. J. Chem. Stud., 2: 12–21.
42. Hsieh S-H, Ting J-M. Characterization and photocatalytic performance of ternary Cu-doped ZnO/Graphene materials. Applied Surface Science. 2018;427:465-75.
43. Saravanan R, Karthikeyan S, Gupta VK, Sekaran G, Narayanan V, Stephen A. Enhanced photocatalytic activity of ZnO/CuO nanocomposite for the degradation of textile dye on visible light illumination. Materials Science and Engineering: C. 2013;33(1):91-8.
44. Oda AM, Ali HH, Lafta AJ, Esmael HA, Jameel AA, Mohammed AM, et al. Study Self-cleaning of Congo Red from Cotton Fabric Loaded by Zno-Ag. International Journal of Chemistry. 2015;7(2).
45. Černík M, Thekkae Padil VV. Green synthesis of copper oxide nanoparticles using gum karaya as a biotemplate and their antibacterial application. International Journal of Nanomedicine. 2013:889.
46. Bhattacharya P, Dhibar S, Hatui G, Mandal A, Das T, Das CK. Graphene decorated with hexagonal shaped M-type ferrite and polyaniline wrapper: a potential candidate for electromagnetic wave absorbing and energy storage device applications. RSC Advances. 2014;4(33):17039.
47. Lu P, Zhou W, Li Y, Wang J, Wu P. Abnormal room temperature ferromagnetism in CuO/ZnO nanocomposites via hydrothermal method. Applied Surface Science. 2017;399:396-402.
48. Molla MAI, Furukawa M, Tateishi I, Katsumata H, Kaneco

S. Fabrication of Ag-doped ZnO by mechanochemical combustion method and their application into photocatalytic Famotidine degradation. Journal of Environmental Science and Health, Part A. 2019;54(9):914-23.
49. Kumari V, Yadav S, Jindal J, Sharma S, Kumari K, Kumar N. Synthesis and characterization of heterogeneous ZnO/CuO hierarchical nanostructures for photocatalytic degradation of organic pollutant. Advanced Powder Technology. 2020;31(7):2658-68.
50. Kaneco S, Li N, Itoh K-k, Katsumata H, Suzuki T, Ohta K. Titanium dioxide mediated solar photocatalytic degradation of thiram in aqueous solution: Kinetics and mineralization. Chemical Engineering Journal. 2009;148(1):50-6.
51. Molla MAI, Ahsan S, Tateishi I, Furukawa M, Katsumata H, Suzuki T, et al. Degradation, Kinetics, and Mineralization in Solar Photocatalytic Treatment of Aqueous Amitrole Solution with Titanium Dioxide. Environmental Engineering Science. 2018;35(5):401-7.
52. Yang X, Qiu L, Luo X. ZIF-8 derived Ag-doped ZnO photocatalyst with enhanced photocatalytic activity. RSC Advances. 2018;8(9):4890-4.
53. Nandi P, Das D. Photocatalytic degradation of Rhodamine-B dye by stable ZnO nanostructures with different calcination temperature induced defects. Applied Surface Science. 2019;465:546-56.
54.Koffyberg, F.P. and F. A. Benko, 1982. A photoelectrochemical determination of the position of the conduction and valence band edges of p-type CuO. J. Appl. Phys., 53: 1173. Singh, J. and R.K. Soni, 2020. Controlled synthesis of CuO decorated defect enriched ZnO nanoflakes for improved sunlight-induced photocatalytic degradation of organic pollutants. Applied Surface Science, 521: 146420.
55. Chen C, Liu X, Fang Q, Chen X, Liu T, Zhang M. Self-assembly synthesis of CuO/ZnO hollow microspheres and their photocatalytic performance under natural sunlight. Vacuum. 2020;174:109198.
56. Sahu K, Bisht A, Kuriakose S, Mohapatra S. Two-dimensional CuO-ZnO nanohybrids with enhanced photocatalytic performance for removal of pollutants. Journal of Physics and Chemistry of Solids. 2020;137:109223.
57. Muzakki A, Shabrany H, Saleh R. Synthesis of ZnO/CuO and TiO2/CuO nanocomposites for light and ultrasound assisted degradation of a textile dye in aqueous solution. Author(s); 2016.
58. Fouda A, Salem SS, Wassel AR, Hamza MF, Shaheen TI. Optimization of green biosynthesized visible light active CuO/ZnO nano-photocatalysts for the degradation of organic methylene blue dye. Heliyon. 2020;6(9):e04896.
59. Ruan S, Huang W, Zhao M, Song H, Gao Z. A Z-scheme mechanism of the novel ZnO/CuO n-n heterojunction for photocatalytic degradation of Acid Orange 7. Materials Science in Semiconductor Processing. 2020;107:104835.
60. Cao F, Wang T, Ji X. Enhanced visible photocatalytic activity of tree-like ZnO/CuO nanostructure on Cu foam. Applied Surface Science. 2019;471:417-24.
61. Pal S, Maiti S, Maiti UN, Chattopadhyay KK. Low temperature solution processed ZnO/CuO heterojunction photocatalyst for visible light induced photo-degradation of organic pollutants. CrystEngComm. 2015;17(6):1464-76.
62. Senthil Kumar P, Selvakumar M, Ganesh Babu S, Induja S, Karuthapandian S. CuO/ZnO nanorods: An affordable efficient p-n heterojunction and morphology dependent photocatalytic activity against organic contaminants. Journal of Alloys and Compounds. 2017;701:562-73.
63. Asif SAB, Khan SB, Asiri AM. Efficient solar photocatalyst based on cobalt oxide/iron oxide composite nanofibers for the detoxification of organic pollutants. Nanoscale Research Letters. 2014;9(1).
64.Pare, B., D. Raghuvanshi, R. Dixit and D. Swami, 2013. Decolorization and mineralization of hazardous brilliant cresyl blue dye utilizing visible light and TiO_2 as photocatalys. Int. J. Chem. Sci., 11(4): 1876-1890.
65. Al-Gubury HY, Alteemi HS, Saad AM, Al-Shamary RR. Removal of Hazardous Brilliant Cresyl Blue Dye Utilizing Aluminum Oxide as Photocatalyst. Indonesian Journal of Chemistry. 2019;19(2):292.
66. Asif SAB, Khan SB, Asiri AM. Visible light functioning photocatalyst based on Al2O3 doped Mn3O4 nanomaterial for the degradation of organic toxin. Nanoscale Research Letters. 2015;10(1).
67.Al-Gubury H.Y. and G.S. Al – Murshidy, 2015. Photocatalytic decolorization of brilliant cresyl blue using Zinc oxide. Int. J. PharmTech Res., 8(2): 289-297.
68.Swami, D., B. Pare and P. Pandit, 2016. Decolorization and mineralization of hazardous brilliant cresyl blue dye using visible light and TiO_2 as photocatalyst. Nature Environment and Pollution Technology, 15(1): 123-128.